Enhanced spin-precession dynamics in a spin-metamaterial coupled resonator observed in terahertz time-domain measurements

T. Kurihara,[1] K. Nakamura,[1] K. Yamaguchi,[1] Y. Sekine,[2] Y. Saito,[2] M. Nakajima,[2,3] K. Oto,[2] H. Watanabe,[1] and T. Suemoto[1]

[1]*Institute for Solid State Physics, The University of Tokyo, 5-1-5 Kashiwanoha, Kashiwa-shi, Chiba 277-8581, Japan*

[2]*Department of Physics, Graduate School of Science, Chiba University, 1-33 Yayoi-cho, Inage-ku, Chiba 263-8522, Japan*

[3]*Institue of Laser Engineering, Osaka University, Suita, Osaka 565-0871, Japan*

(Received 22 May 2014; published 6 October 2014)

We demonstrate enhancement of the spin precession of orthoferrite $ErFeO_3$ using the magnetic near-field produced by a split-ring resonator (SRR), using the terahertz pump-optical Faraday probe measurement. The precession amplitude was enhanced by ∼8 times when the resonance frequency of spin precession was close to the magnetic resonance of SRR. The time evolution of spin precession was successfully reproduced by a coupled spin- and SRR-resonance model mediated by the magnetic near-field. It is suggested that optimization of the metamaterial structure would further increase the enhancement factor, leading to the nonlinear control of spin dynamics using terahertz radiation.

DOI: 10.1103/PhysRevB.90.144408 PACS number(s): 78.66.Bz, 42.60.Da, 75.78.Jp, 78.20.Ls

Ultrafast optics techniques enable the spin dynamics to be controlled with a temporal resolution of picoseconds to femtoseconds, which is unachievable with conventional electronics-based methods. Such techniques are receiving increasing attention both for the fundamental science and spintronics applications [1–6]. Various methods have been proposed and demonstrated, such as the inverse Raman effect [1,2], optical pumping [3,6], thermal demagnetization [4,5], etc. In contrast to these visible-light-based spin manipulation methods, direct spin manipulation using the magnetic field of terahertz (THz) radiation is particularly useful because it can trigger spin precession on the timescale of subpicoseconds without accompanying unwanted electronic excitation or thermal effects [7–10].

Another important topic related to the dynamic magnetic responses in the THz frequency is metamaterial technology, which uses the subwavelength metallic structures as local magnetic oscillators [11–15]. Such structures have the ability to create a strongly enhanced magnetic near-field in the vicinity of the structures. By using such a locally enhanced magnetic field, we can expect to greatly increase the amplitude of the spin precession. The metamaterial-enhanced "electric" field has been utilized to induce strong nonlinear effects such as a metal-insulator transition in VO_2 [16] and impact ionization in semiconductors [17], etc., but in contrast to these remarkable successes with the "electric" field, the utilization of the enhanced "magnetic" field is still limited. The stationary transmission measurement of electron spin resonance in the presence of split-ring resonator (SRR) metamaterials has been reported [18], but the dynamics of the coupled spin-metamaterial system in the time domain are still unrevealed.

In this paper, we demonstrate the excitation of spin precession by an enhanced magnetic field of SRR and reveal the dynamical behavior in the time domain using the THz pump-optical probe setup. We observed that the spin-precession amplitude was enhanced by a factor of ∼8 due to the magnetic coupling with the SRR. Furthermore, we successfully describe the temporal dynamics of the spin-SRR coupled system in terms of a simple model considering the spin equation of motion and an inductor-capacitor-resistor (LCR) circuit. The result suggests the scalability of the method for obtaining higher levels of magnetic-field enhancement.

A schematic of the experimental configuration is shown in Fig. 1. We fabricated the SRR structure on the surface of a 130-μm-thick, c-cut single crystal of erbium orthoferrite ($ErFeO_3$), grown by the floating zone method. The crystal axes were determined from x-ray Laue diffraction. $ErFeO_3$ is a canted antiferromagnet, in which antiferromagnetically ordered Fe^{3+} spins cant toward one direction and form macroscopic magnetization [19]. In the temperature range below the spin reorientation transition ($\leqslant$87 K), the macroscopic magnetization is in a direction parallel to the a axis of the crystal [20]. In the sub-THz frequency, it is known to have two magnetic resonance modes, namely, the quasiferromagnetic (F) mode and the quasiantiferromagnetic (AF) mode [21]. The F mode can be interpreted as the precession of macroscopic magnetization around its easy axis, while the AF mode can be viewed as its stretching vibration. In our experiment, we focus on the behavior of the F mode, the frequency of which is known to depend strongly on temperature [10,22]. Thus, a change in the temperature will allow the frequency of spin precession to be tuned around the SRR resonance.

The SRR structure under study was fabricated by the electron beam lithography technique, is made of aluminum, and has a lateral dimension of 60 μm × 60 μm, thickness of ∼200 nm, line width of 10 μm, and gap width of 10 μm. The gap of SRR was parallel to the b axis. The resonance frequency of the magnetic mode predicted from finite-difference time-domain calculation is ∼0.22 THz. The THz pulse was generated by the Cherenkov optical rectification technique [23,24] using a $LiNbO_3$ nonlinear optical crystal, pumped by a Ti:sapphire regenerative amplifier with an energy of ∼4 mJ/pulse, a repetition rate at 1 kHz, pulse width of ∼100 fs, and central wavelength of ∼800 nm. The generated THz pulse had a half-cycle waveform, peak electric- and magnetic-field amplitude of ∼240 kV/cm and ∼0.07 Tesla, respectively, and central frequency of ∼0.5 THz. The spin precession was measured in the time domain by Faraday rotation of an 800 nm probe pulse transmitted through the sample, as explained later. The diameters of the THz and probe spots were ∼1 mm

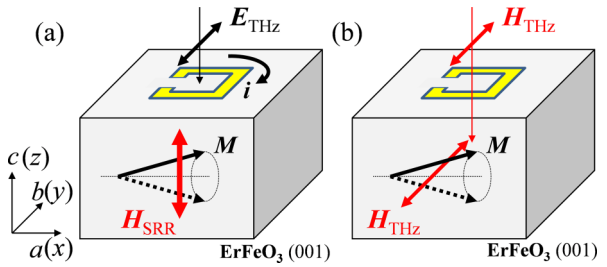

FIG. 1. (Color online) Schematic of the experimental configuration. (a) Excitation of spin precession with magnetic near-field of an SRR induced by a THz electric field and (b) direct excitation of spin with a THz magnetic field.

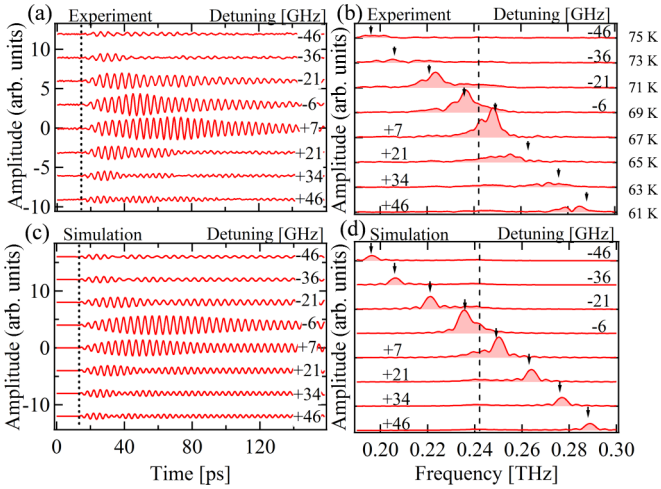

FIG. 2. (Color online) (a) Temperature dependence of the Faraday waveforms obtained from the experiment. (b) Fourier transform of (a). (c) Waveforms simulated using Eqs. (1.1)–(1.4). (d) Fourier transform of (c). Black arrows in (b) and (d) indicate the resonance frequency of spin at each detuning. The parameters used in the calculation are: $|\boldsymbol{M}_1| = 1 \times 10^{-16}$ [Wb m], $m_1 = 6 \times 10^{13}$ [m^{-1}], $s_1 = -1 \times 10^{14}$ [$H^{-1}m^{-1}$], $\gamma = 2.2 \times 10^5$ [$m\,s^{-1}\,A^{-1}$], $\alpha = 0.025$, $L = 3.3 \times 10^{-11}$ [H], $C = 1.33 \times 10^{-14}$ [F], $R = 2[\Omega]$, respectively. Dotted lines in (b) and (d) show the resonance frequency of the SRR.

and ~30 μm, respectively. The position of the probe spot on the sample surface was monitored by a charge-coupled device camera. The experiments were performed with two mutually orthogonal incident THz polarizations. In the first experiment [Fig. 1(a)], the electric and magnetic fields of the THz radiation were parallel to the b and a axes of the crystal, respectively (SRR-excitation polarization). Owing to the broken symmetry of the SRR structure, the incidence of the THz pulse with electric field polarized parallel to the gap of the SRR induces a circulating current in SRR [14]. In this polarization, the magnetic-field component of the incident THz pulse does not directly excite the spin precession. The circulating current in the SRR produces an enhanced magnetic near-field polarized along the c axis, which causes the $ErFeO_3$ spins to precess around the a axis. Because of the precession, a magnetization component parallel to the c axis appears, which can be detected via optical Faraday rotation of the visible probe. In the second experiment, the polarization of the incident THz pulse was rotated by 90° [Fig. 1(b); spin-excitation polarization]. Under these conditions, the electric-field component of the THz pulse does not excite the SRR, but the magnetic component directly excites spin precession. In this way, we can selectively excite either the SRR or spin by choosing the polarization of the THz pulse.

Figures 2(a) and 2(b), shows the temporal waveforms and Fourier spectra of the Faraday signal, respectively, obtained from the first experiment using SRR-excitation polarization. The resonance frequency of spin was swept from ~0.20 to ~0.29 THz by changing the temperature from 75 to 61 K [10,22]. The THz pulse is incident on the sample at $t = 13$ ps. The rise and decay times observed in Fig. 2(a) depend on the temperature or detuning from the SRR resonance frequency. When the frequency of spin resonance was close to that of the SRR (69 K and 67 K), we observed a longer rise time and a substantial increase in the precession amplitude. The corresponding Fourier spectrum revealed that the amplitude was a maximum around this resonance frequency, indicating clearly that the spin was resonantly excited by the magnetic near-field of the SRR. When the SRR frequency was far from that of the spin resonance, we observed a smaller signal amplitude and beating of the spin oscillation in the earlier periods of the time evolution. For example, at $t = 20$–80 ps, the +39 GHz-detuned waveform in Fig. 2(a) exhibits the beating with an ~25 ps period. Close observation of the Fourier spectrum reveals that in addition to the main peak of the spin precession (~0.285 THz), there is a weak peak at ~0.248 THz, which corresponds to the resonance frequency of the SRR. The beating period of ~25 ps (~40 GHz) corresponds to the detuning, or the frequency difference between the main peak (~0.285 THz) and SRR peak (~0.248 THz).

$$\frac{d\boldsymbol{M}_1}{dt} = -\gamma \boldsymbol{M}_1 \times \boldsymbol{H}_{\mathrm{eff},1} + \frac{\alpha}{|\boldsymbol{M}_1|}\boldsymbol{M}_1 \times \frac{d\boldsymbol{M}_1}{dt} \tag{1.1}$$

$$L\frac{d^2 i(t)}{dt^2} + R\frac{di(t)}{dt} + \frac{1}{C}i(t) = \frac{dE(t)}{dt} \tag{1.2}$$

$$E(t) = E_{\mathrm{THz},y}(t) + m_1 \frac{dM_{1z}(t)}{dt} \tag{1.3}$$

$$\boldsymbol{H}_{\mathrm{eff},1}(t) = s_1 L i(t)\hat{\boldsymbol{z}} + H_0\hat{\boldsymbol{x}} + H_{\mathrm{THz}}(t)\hat{\boldsymbol{y}} \tag{1.4}$$

To understand the spin-precession behavior in more detail, we constructed a model based on the Landau-Lifshitz-Gilbert (LLG) equation to describe the spin dynamics [Eq. (1.1)], magnetically coupled to an LCR circuit, which expresses the SRR [Eq. (1.2)]. The coordinates of x, y, and z correspond to the a, b, and c axes of the crystal, respectively. The resistance R was estimated from the conductivity of aluminum [25], while inductance L and capacitance C were determined from the resonance frequency of SRR and its quality (Q) factor obtained from Fig. 2(b). The current $i(t)$ is driven by an external force $E(t)$ that consists of an incident THz electric-field pulse $E_{\mathrm{THz},y}(t)$ and the electromotive force $m_1 \cdot dM_{1z}(t)/dt$ caused by the oscillation of the magnetic moment inside the SRR. On the other hand, the magnetic moment $\boldsymbol{M}(t)$ is driven by a magnetic field generated by the current $i(t)$ in the LCR circuit [Eq. (1.4)]. Here, the y component of the incident magnetic field of the THz pulse $H_{\mathrm{THz}}(t)$ is zero. The parameter H_0

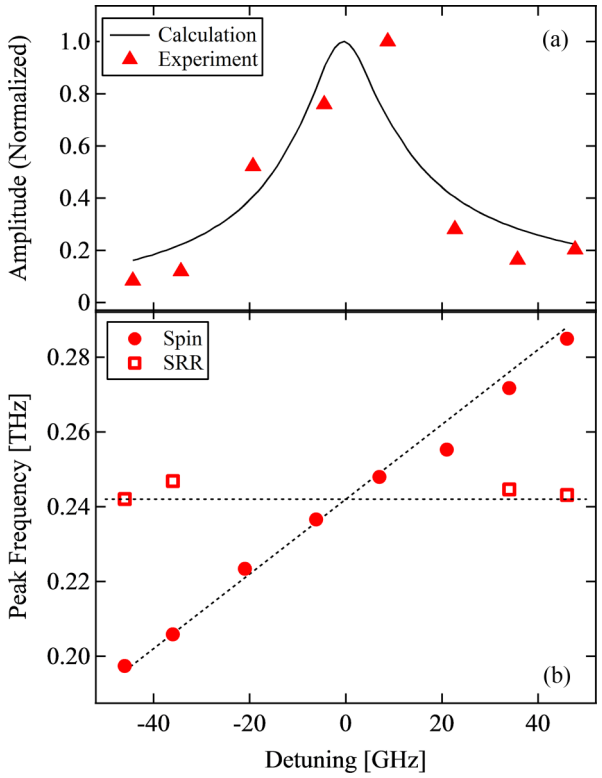

FIG. 3. (Color online) (a) Peak amplitude of spin precession obtained from the experiment (red triangles) and calculation (black solid curve). (b) Experimental peak frequencies of the spin resonance (red circles) and SRR resonance (red squares) as a function of detuning. The black dotted lines show the corresponding set frequencies used in the calculation.

expresses the (static) anisotropy field of the $ErFeO_3$ crystal and determines the resonance frequency of spin precession. The parameters s_1 and m_1 determine the strength of the coupling of the field to the oscillator. Figure 2(c) shows the time evolution of the x component of the magnetization $M_{1z}(t)$ calculated using the presented model. Their Fourier spectra are shown in Fig. 2(d). The parameter H_0 was varied to tune the frequency of spin precession around the SRR resonance ($H_0 = 6.9 \times 10^6$ A/m at resonance). The result shows a good agreement with waveforms obtained in the experiment.

The amplitude and peak frequency of the spin precession are shown as a function of detuning frequency in Figs. 3(a) and 3(b), respectively. The black solid curve is the simulation result, and markers are the experiment. The increase of spin-precession amplitude near the SRR resonance frequency is clearly reproduced in Fig. 3(a), reaching up to 8 times stronger than at the off-resonance frequencies. This enhancement factor is of the same order as what was calculated from the finite-difference time-domain (FDTD) simulation (~10 times at the center of SRR). It is slightly smaller than the simulation, probably because the observed precession amplitude is the averaged signal within the finite size of the probe spot, which includes lower amplitude regions. It is worth noting that near the SRR resonance frequency, the precession amplitude measured inside an SRR was about an order stronger than that outside the SRR, which also confirmed that the magnetic field was locally enhanced by the SRR compared to the incident THz radiation. Here, the spectral width of the enhancement curve is determined mainly by the Q factor of the SRR. The anticrossing of the precession frequency was not resolved in Fig. 3(b), probably because the splitting caused by the spin-SRR coupling was small compared to the SRR resonance line width in our case [18].

Next, to investigate the coupling behavior of spin and SRR at resonance, we measured the spin precession with the incident THz polarization in a spin-excitation configuration. As mentioned earlier, the magnetic field of a THz pulse directly excites the spin precession in this polarization without exciting the SRR. Here, we tuned the frequency of the spin resonance near the SRR resonance by setting the temperature to 69 K.

The resulting waveform is shown in Fig. 4(a), along with the waveform obtained in the first experiment at the same temperature for comparison. The clearest difference in the two waveforms can be seen in their lifetimes. While the SRR-excited precession decays within $\leqslant$160 ps, the spin-excited precession lasts for over ~300 ps. This 300 ps lifetime matches the lifetime measured at a position without the SRR; in other words, the coupling with SRR seems to shorten the lifetime of the original spin precession. As will be explained later, within the aforementioned model, this short lifetime of 160 ps is dominated by the Joule energy loss of the SRR, and it is independent of the polarization of the incident THz pulse. The long lifetime observed in the spin-excitation case suggests the existence of a spin weakly interacting with the SRR. In the spin-excitation polarization, the spins in the deeper region of the sample, which is unaffected by the SRR on the surface, can be excited uniformly by the incident THz pulse, and such spins should exhibit a weaker coupling with the SRR than those at the surface [26]. (Note that the depth where the magnetic near-field of SRR is influential [~20 μm in our case] is much shorter than the thickness of the crystal sample [130 μm].) Therefore, we extended our coupled LLG-LCR equation model to introduce the second spin, which has a different coupling strength with the SRR from the first one. We thus added the following equations to Eq. (1.1)–(1.4):

$$\frac{d\boldsymbol{M}_2}{dt} = -\gamma \boldsymbol{M}_2 \times \boldsymbol{H}_{\mathrm{eff},2} + \frac{\alpha}{|\boldsymbol{M}_2|}\boldsymbol{M}_2 \times \frac{d\boldsymbol{M}_2}{dt} \tag{2.1}$$

$$\boldsymbol{H}_{\mathrm{eff},2}(t) = s_2 Li(t)\hat{\boldsymbol{z}} + H_0\hat{\boldsymbol{x}} + H_{\mathrm{THz}}(t)\hat{\boldsymbol{y}} \tag{2.2}$$

and we replaced Eq. (1.3) with:

$$E(t) = E_{\mathrm{THz},y}(t) + m_1\frac{dM_{1z}(t)}{dt} + m_2\frac{dM_{2z}(t)}{dt} \tag{2.3}$$

Here, $\boldsymbol{M}_2$ describes the spin component with weaker coupling with the SRR than $\boldsymbol{M}_1$. We should also note that the lateral nonuniform distribution of the magnetic near-field in the SRR may also result in a variation of the coupling constant.

The calculation results for the cases of SRR-excitation and spin-excitation polarizations are shown in Figs. 4(b) and 4(c), respectively. The parameters used in the simulation are shown in the caption of Fig. 4. In (b), we see that the amplitudes of $\boldsymbol{M}_1$ and $\boldsymbol{M}_2$ are quite different. Because the spins are excited only by the magnetic field produced by the SRR in this polarization,

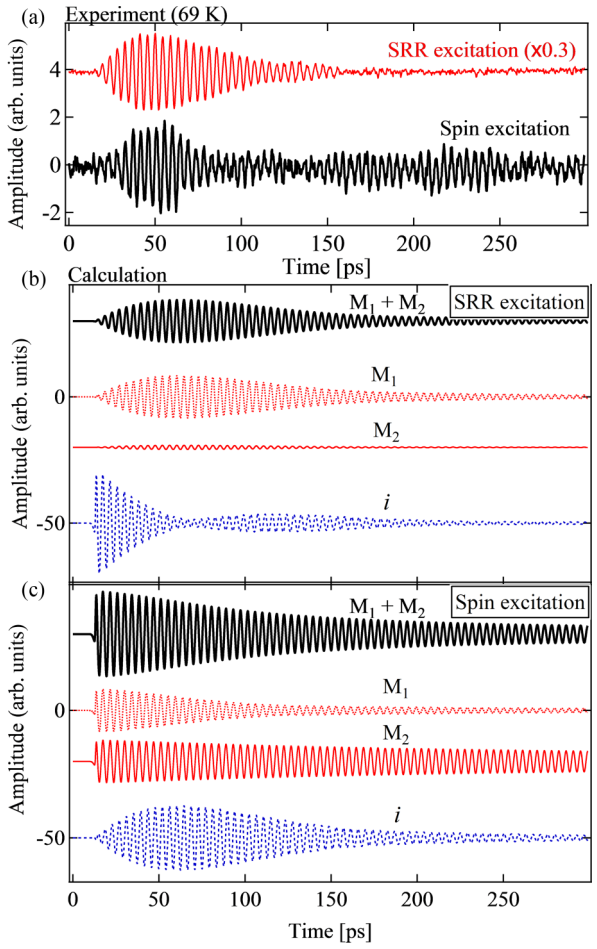

FIG. 4. (Color online) (a) THz temporal waveforms obtained at 69 K with SRR-excitation (red) and spin-excitation polarization (black solid). (b) and (c) Waveforms calculated from the coupled LLG-LCR equation assuming two spins and (b) SRR-excitation polarization or (c) spin-excitation polarization. The total magnetization ($\boldsymbol{M}_1 + \boldsymbol{M}_2$; black), the z component of the spin with the stronger coupling constant with the SRR ($\boldsymbol{M}_1$; red dotted), the spin with the weaker coupling ($\boldsymbol{M}_2$; red solid), and the current (i; blue dashed) in the SRR are all shown. Parameters used in the calculation are: $|\boldsymbol{M}_1| = 1 \times 10^{-16}$ [Wb m], $|\boldsymbol{M}_2| = 1 \times 10^{-16}$ [Wb m], $m_1 = 6 \times 10^{13}$ [m^{-1}], $m_2 = 6 \times 10^{12}$ [m^{-1}], $s_1 = -1 \times 10^{14}$ [H^{-1}m^{-1}], $s_2 = -1 \times 10^{13}$ [H^{-1}m^{-1}], $H_0 = 6.8 \times 10^6$ [A m^{-1}], respectively. Other parameters are the same as in Fig. 2.

only the spin that is strongly coupled to the SRR ($\boldsymbol{M}_1$) can be excited effectively, while the spin with weak coupling ($\boldsymbol{M}_2$) cannot. Therefore, in the SRR-excitation case, the dynamics of macroscopic magnetization are dominated by the strongly coupled spin $\boldsymbol{M}_1$. The short lifetime of $\boldsymbol{M}_1$ ($\sim$160 ps) can be explained by examining the time evolution of the current $i(t)$: As the THz electric pulse is incident on the SRR at $t = 13$ ps, the current i starts to oscillate in the SRR. Because the SRR is strongly coupled to $\boldsymbol{M}_1$ near the resonance frequency, the energy stored in the SRR flows into the spin system until i reaches zero and $\boldsymbol{M}_1$ is a maximum (at $t \sim 60$ ps). Following this, i revives, because the energy stored in the spin system flows back into the SRR owing to the electromotive force. After that, both i and $\boldsymbol{M}_1$ decrease with a similar decay constant ($\sim$100 ps), determined by the Joule energy loss in the SRR. The agreement of calculated M_1 waveform with the experimental waveform indicates that the observed lifetime is determined by such a bidirectional energy-flow mechanism. In contrast, in the spin-excitation case [Fig. 4(c)], because both M_1 and M_2 are excited simultaneously, the amplitudes of the precession for both spins are comparable, but the lifetimes of M_1 and M_2 are quite different. The shorter lifetime of M_1 ($\leqslant$100 ps) can be explained using the same energy-flow argument, whereas the longer lifetime of the weakly coupled spin M_2 is a result of the energy stored in M_2 flowing into the SRR at a much slower rate. In summary, the long lifetime of the spin-excitation signal is dominated mainly by the weakly coupled spin M_2, while the short lifetime of the SRR-excitation signal is determined by the strongly coupled spin M_1, reflecting the Joule energy loss of the SRR. Thus, we can explain the polarization dependence of the observed lifetimes by considering the two-spin model.

In conclusion, we studied the spin-precession dynamics in orthoferrite $ErFeO_3$ magnetically coupled to the resonance of SRR using a THz pump-optical probe setup, and we observed spin-precession enhancement by $\sim$8 times at maximum. Through polarization measurement and numerical calculation using a coupled LLG-LCR equation, it has been shown that bidirectional energy flow between spin precession and SRR resonance mediated by a magnetic field is essential in understanding the dynamical behavior of spin precession. Our results indicate that the magnetic near-field in SRR can enhance the precession by about an order of magnitude. Adjusting the design of metamaterial may allow the field to be enhanced even further and lead to the realization of nonlinear spin control using THz radiation.

This work was supported by Japan Society for the Promotion of Science KAKENHI Grants No. 23244063, No. 26287060, No. 25286063, and No. 24656043, and Nippon Sheet Glass Foundation for Materials Science and Engineering.

[1] A. V. Kimel, A. Kirilyuk, and T. Rasing, Laser Photon. Rev. **1**, 275 (2007).
[2] A. V. Kimel, A. Kirilyuk, P. A. Usachev, R. V. Pisarev, A. M. Balbashov, and Th. Rasing, Nature **435**, 655 (2005).
[3] R. Akimoto, K. Ando, F. Sasaki, S. Kobayashi, and T. Tani, J. Appl. Phys. **84**, 6318 (1998).
[4] A. V. Kimel, A. Kirilyuk, A. Tsvetkov, R. V. Pisarev, and Th. Rasing, Nature **429**, 850 (2004).
[5] J. A. de Jong, I. Razdolski, A. M. Kalashnikova, R. V. Pisarev, A. M. Balbashov, A. Kirilyuk, Th. Rasing, and A. V. Kimel, Phys. Rev. Lett. **108**, 157601 (2012).
[6] T. Satoh, Nguyen Phuc Duong, and M. Fiebig, Phys. Rev. B **74**, 012404 (2006).

[7] M. Nakajima, A. Namai, S. Ohkoshi, and T. Suemoto, Opt. Express **18**, 18260 (2010).
[8] K. Yamaguchi, M. Nakajima, and T. Suemoto, Phys. Rev. Lett. **105**, 237201 (2010).
[9] T. Kampfrath, A. Sell, G. Klatt, A. Pashkin, S. Mährlein, T. Dekorsy, M. Wolf, M. Fiebig, A. Leitenstorfer, and R. Huber, Nat. Photonics **5**, 31 (2011).
[10] K. Yamaguchi, T. Kurihara, Y. Minami, M. Nakajima, and T. Suemoto, Phys. Rev. Lett. **110**, 137204 (2013).
[11] J. B. Pendry, A. J. Holden, D. J. Robbins, and W. J. Stewart, IEEE Trans. Microwave Theory Tech. **47**, 2075 (1999).
[12] W. J. Padilla, A. J. Taylor, C. Highstrete, M. Lee, and R. D. Averitt, Phys. Rev. Lett. **96**, 107401 (2006).
[13] X. G. He, C. L. Hsueh, and J. Q. Shi, Phys. Rev. Lett. **84**, 18 (2000).
[14] C. M. Soukoulis, T. Koschny, J. Zhou, M. Kafesaki, and E. N. Economou, Phys. Status Solidi B **244**, 1181 (2007).
[15] K. Fan, A. C. Strikwerda, H. Tao, X. Zhang, and R. D. Averitt, Opt. Exp. **19**, 12619 (2011).
[16] M. Liu, H. Y. Hwang, Hu Tao, A. C. Strikwerda, K. Fan, G. R. Keiser, A. J. Sternbach, K. G. West, S. Kittiwatanakul, J. Lu, S. A. Wolf, F. G. Omenetto, X. Zhang, K. A. Nelson, and R. D. Averitt, Nature **487**, 345 (2012).
[17] K. Fan, H. Y. Hwang, M. Liu, A. C. Strikwerda, A. Sternbach, J. Zhang, X. Zhao, X. Zhang, K. A. Nelson, and R. D. Averitt, Phys. Rev. Lett. **110**, 217404 (2013).
[18] A. Schneider, A. Shuvaev, S. Engelbrecht, S. O. Demokritov, and A. Pimenov, Phys. Rev. Lett. **103**, 103907 (2009).
[19] S. M. Shapiro, J. D. Axe, and J. P. Remeika, Phys. Rev. B **10**, 2014 (1974).
[20] R. L. White, J. Appl. Phys. **40**, 1061 (1969).
[21] G. F. Herrmann, J. Phys. Chem. Solids **24**, 597 (1963).
[22] G. V. Kozlov, S. P. Lebedev, A. A. Mukhin, A. S. Prokhorov, I. V. Fedorov, A. M. Balbashov, and I. Y. Parsegov, IEEE Trans. Magn. **29**, 3443 (1993).
[23] J. A. Fülöp, L. Pálfalvi, G. Almási, and J. Hebling, Opt. Exp. **18**, 12311 (2010).
[24] H. Hirori, A. Doi, F. Blanchard, and K. Tanaka, Appl. Phys. Lett. **98**, 091106 (2011).
[25] M. A. Ordal, R. J. Bell, R. W. Alexander, Jr., L. L. Long, and M. R. Querry, Appl. Opt. **24**, 4493 (1985).
[26] N. Kumar, A. C. Strikwerda, K. Fan, X. Zhang, R. D. Averitt, P. C. M. Planken, and A. J. L. Adam, Opt. Exp. **20**, 11277 (2012).